Multiscale Structures and Their Evolution in a Screen Cylinder Wake

Azlin M. Azmi, T. Zhou, A. Rinoshika, L. Cheng

Abstract—The turbulent structures in the wake (x/d =10 to 60) of a screen cylinder have been educed to understand the roles of the various structures as evolving downstream by comparing with those obtained in a solid circular cylinder wake at Reynolds number, Re of 7000. Using a wavelet multiresolution technique, the flow structures are decomposed into a number of wavelet components based on their central frequencies. It is observed that in the solid cylinder wake, large-scale structures (of frequency f_0 and 1.2 f_0) make the largest contribution to the Reynolds stresses although they start to lose their roles significantly at x/d > 20. In the screen cylinder wake, the intermediate-scale structures ($2f_0$ and $4f_0$) contribute the most to the Reynolds stresses at x/d =10 before being taken over by the large-scale structures (f_0) further downstream.

Keywords—Turbulent structure, screen cylinder, vortex, wavelet multiresolution analysis.

I. INTRODUCTION

THE solid cylinder wakes are characterized by organized vortex structures when Reynolds number Re is higher than 49, where the Reynolds number, Re, is defined as $U_\infty d/\nu$, with d being the diameter of the cylinder, U_∞ the free stream and ν the kinematic viscosity of the fluid. As vortices are shed regularly and alternatively from the cylinder, periodic drag (force parallel to the flow) and lift (force perpendicular to the flow) are generated, which may lead to Vortex-Induced Vibrations (VIV). VIV of cylindrical structures should be avoided as it will lead to fatigue damage. In this context, extensive studies have been conducted to understand the physics of this kind of flow at various range of Re due to its widespread applications in engineering (for example in the design of offshore structures, heat exchanger, bridges, transmission lines and aircraft control surfaces).

VIV can be suppressed using passive methods [1]. Perforated shroud is one of these, which are effective in perturbing vortex shedding. Price [2] tested the vibration response of shrouded cylinders with different shroud configurations of 37% porosity at $Re = 4640$. It was found that all the shrouds were overall effective for the range of the

A. M. Azlin is with the School of Civil and Resource Engineering, University of Western Australia, 35 Stirling Highway, 6009 WA, Australia (phone: 618-6488-1733; e-mail: ceklin167@yahoo.com).

T. Zhou is with the School of Civil and Resource Engineering, University of Western Australia, 35 Stirling Highway, 6009 WA, Australia (phone: 618-6488-7094; e-mail: tongming.zhou@uwa.edu.au).

A. Rinoshika is with the Department of Mechanical Systems Engineering, Yamagata University, 4-3-16 Jonan, Yonezawa-shi, 992-8510, Japan (e-mail: rinosika@yz.yamagata-u.ac.jp).

L. Cheng is with the School of Civil and Resource Engineering, University of Western Australia, 35 Stirling Highway, 6009 WA, Australia (phone: 618-6488-3076; e-mail: liang.cheng@uwa.edu.au).

tested spring stiffness k although they were less effective for low spring stiffness. The effectiveness in VIV suppression was markedly improved at higher stiffness by reducing the vibrational double-amplitude up to about 97%. Zdravkovich and Volk [3] extended the shroud test to high reduced velocities (beyond synchronization range) for three types of shroud, namely, the square-holed, circular-holed and a fine-mesh gauze all having 36% porosity. They found that the shroud made of fine-mesh gauze (with wire diameter of 0.102 mm and hole size of 0.152 mm) was the most effective in suppressing the vibration of a cylinder, giving the highest reduction in the double-amplitude of vibration.

In a recent study [4], the effectiveness of a screen cylinder in VIV reduction was investigated and the result showed that the vibration of a plain cylinder was reduced by about 50%. The screen cylinder wake was also studied in the near-wake and compared with a plain solid cylinder wake using a phase-averaged technique which decomposes turbulent signals into coherent and incoherent structures according to their energy and phase values respectively. Significant differences of flow structures and momentum transport characteristics between the solid cylinder and the screen cylinder wakes were observed. It would also be interesting to understand the effect of the intermediate-scale as well as the relatively small-scale structures on the wake dynamics and the role these structures play. In this context, wavelet analysis can be used, which decomposes the turbulent signals into different levels and allows the measured time-frequency data to be analyzed in time-domain, frequency-domain and a combination of the above, which cannot be done by the other techniques [5]-[7].

Recently, Rinoshika, and Zhou [8] developed a one-dimensional orthogonal wavelet multiresolution technique to study the turbulent structures of various scales in the near wake of a circular cylinder. This technique allows separation of the flow into a number of wavelet components based on their central frequencies. These different central frequencies represent structures of different scales. The dependence of these structures on various bluff bodies (circular cylinder, screen strip, square cylinder, triangular cylinder) in both the near and far wakes of these bodies were further examined [9]-[11]. In addition, the multiresolution technique was also used to examine the velocity and vorticity characteristics in the wake generated by an inclined circular cylinder [12].

The main objectives of the present work are to clarify the role of the turbulent structures other than the organized large-scale structures and their evolution in the streamwise direction in the screen cylinder wake. The wavelet analysis technique is used to decompose the data into a number of subsets based on

World Academy of Science, Engineering and Technology
International Journal of Mechanical and Mechatronics Engineering
Vol:8, No:2, 2014

their characteristics central frequencies or scales. The screen cylinder wake is compared with that of a solid cylinder wake (and the screen strip wake, accordingly) in terms of the behavior from different subsets.

II. EXPERIMENTAL DETAILS

The experiments were conducted in a blower type wind tunnel with a test section of 380mm (width) x 255mm (height) and 1.8m long. All interior surfaces of the test section were made of smooth acrylic to minimize any boundary layer effects. The free stream velocity in the test section was uniform to 0.2%, and the longitudinal turbulence intensity was less than 0.5%. A solid circular cylinder and a screen cylinder were used to generate the turbulent wake. Both of them have an outer diameter d of 23mm and a length l of 380mm, giving an aspect ratio of $l/d = 16.5$. The solid cylinder was a plain, smooth cylinder made of polished aluminium. The screen cylinder was made of a stainless steel mesh of square-cross-section with porosity of $\beta = 67\%$. The diameter of the mesh wire is 0.45mm.

Fig. 1 shows the sketch of the wake profile and the probe arrangement in the experiment. The coordinate system is defined such that the x-axis is in the same direction of the incoming flow, the y-axis is in the vertical plane through the cylinder and normal to the x-axis and the z-axis is normal to both the x and y-axes. All measurements were performed at a free stream velocity U_∞ of 4.57 m/s, corresponding to Re ≈ 7000. For the solid cylinder, measurements were conducted at three downstream locations, i.e., $x/d = 10, 20$ and 40 while for the screen cylinder the measurement locations are at $x/d = 10$ to 60 with an increment of 5. Due to the limitation of the tunnel height and the difficulties in making a cylinder of small diameter reliably, the present experiments could not be conducted in the far wakes particularly for the solid cylinder. A vorticity probe was used to measure the longitudinal and transverse velocity fluctuations, u and v, respectively. The vorticity probe consists of an X-probe straddled by a pair of parallel hot wires (Fig. 1). The probe was moved across the wake in the y-direction. Wire a and b denoted the two inclined wires of the X-probe for u and v measurements while wires c and d denoted the two parallel hot wires for u measurements. Both wires had a separation of 1.6mm.
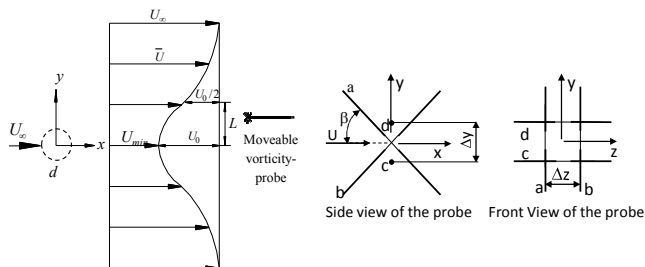

Fig. 1 Wake profile, probe arrangement and schematics of the vorticity probe

The hot wires were etched from Wollaston (Pt-10% Rh) wires with a wire diameter of $5\mu m$. Angle calibration of the X-probe was performed over $\pm 20°$. The effective angles of the inclined wires in the X-probe were 34° and 31°, respectively. The hot wires were operated with in-house constant temperature circuits at an over heat ratio of 1.5. The resistance of each wire ranged between 10-11Ω whereby the output signals were low-pass filtered at a cut-off frequency f_c set at 2.8 kHz. The filtered signals were sampled at a frequency $f_s = 2f_c$ into a PC using a 16-bit A/D converter (National Instrument). The sampling period T_s was 30s. Experimental uncertainties were inferred from the hot-wire calibration data errors as well as the scatter observed in repeating the experiments a number of times. The uncertainty for the time-average velocity, $\bar{U}$ was estimated to be about $\pm 2\%$ while for the fluctuating velocities u and v the uncertainties were about $\pm 5\%$ and $\pm 6\%$ respectively.

III. WAVELET ANALYSIS AND SIGNALS DECOMPOSITION

The present work applies the orthogonal wavelet multiresolution technique and uses the same method as performed by Razali et al. [12] in the turbulent wake of an inclined circular cylinder. The Daubechies family [13] with an order of 20 is chosen as the wavelet basis due to its satisfactory frequency localization. The wavelet decomposition of the velocity signal is done in the following way. An instantaneous velocity component, U (or V), can be written as the sum of a time-averaging component, $\bar{U}$, and a fluctuation component, u, viz.,

$$U = \bar{U} + u \qquad (1)$$

Using the wavelet multiresolution technique, the fluctuation component u is decomposed into a number of orthogonal wavelet components based on the central frequencies/wavelet levels. These central frequencies are directly linked to the turbulent structure scales. The original fluctuation velocity data can be reconstructed by the summation of all fluctuation velocity of each wavelet level as follows

$$u = \sum_{i=1}^{n} u_i \qquad (2)$$

where u_i is the fluctuation velocity component of u at the ith wavelet level and n is the total number of wavelet levels. The instantaneous velocity component as in (2) can also be written as

$$U = \bar{U} + \sum_{i=1}^{n} u_i \qquad (3)$$

The instantaneous wavelet component of velocity in the x- and y-direction, U_i and V_i respectively are therefore written as,

$$U_i = \bar{U} + u_i$$
$$V_i = \bar{V} + v_i \approx v_i \qquad (4)$$

since measurement indicates that $\bar{V} \approx 0$.

World Academy of Science, Engineering and Technology
International Journal of Mechanical and Mechatronics Engineering
Vol:8, No:2, 2014

IV. RESULTS AND DISCUSSIONS

A. The Dominant Frequencies

Prior to the wavelet multiresolution analysis, a dominant frequency of turbulent structures has to be determined. This frequency is selected at the averaging frequency or scale of organized structures obtained from the power spectral density function ϕ_v of the velocity signal v at $y^* = 0.5$, which is approximately on the vortex path. Hereafter, a superscript asterisk denotes normalization by d for the length scale and/or U_∞ for the velocity scale. The v-signal is chosen due to its higher sensitivity in detecting organized structures than the other velocity components. The velocity signals are analyzed by the Fast Fourier Transform method. The power spectral density functions of the measured v–signals (dashed line) for both the solid and the screen cylinder wakes are shown in Figs. 2 and 3, respectively, at different streamwise locations. The spectra of the wavelet components are plotted on the same figure and will be discussed later. The spectra in the solid cylinder wake (Fig. 2) show a distinct peak at the frequency of 41 Hz, corresponding to $f_0^* = f_0 d/U_\infty \approx 0.21$ at all streamwise locations especially in the near wake at $x^* = 10$ and 20. This frequency is known as the vortex shedding frequency or the Strouhal number in a circular cylinder wake as a result of the existence of the large-scale Kármán vortex structures. Thus, the frequency, $f_0 = 41$Hz, is specified as the dominant central frequencies in the solid cylinder wake at all the measured locations. It can be seen that the maximum energy of the measured spectra decreases with x^*, indicating a reduction in the vortex shedding intensity further downstream of the solid cylinder. On the other hand, the spectra of the measured v-signals in the screen cylinder wake (Fig. 3) at $x^* = 10$ displays no apparent peak and only shows a noticeable peak at $x^* \geq 20$ (although less sharp than the solid cylinder spectra), indicating the event of the large-scale vortical structures. The identified dominant frequencies at $x^* = 10$, 20, 30, 40, 50, and 60 in the screen cylinder wake are 66, 56, 54, 52, 53, and 53 Hz, respectively. It can be observed that the peak magnitude increases with downstream distance until $x^* = 40$, thereafter decreases only slightly, indicating a vortex growth trend in the streamwise direction, a complete opposite trend to that of the solid cylinder wake. Note also that the spectra magnitude in the screen cylinder wake decreases significantly (by the order of one-tenth) in comparison to that in the solid cylinder wake implying much weaker vortex strength in the former.

B. Frequency Characteristics of Wavelet Components

The spectral characteristics of each wavelet components are obtained by analyzing the velocity signal v at a location $y^* = 0.5$ using the wavelet multiresolution technique. The velocity signal is decomposed into 17 wavelet levels, i. Figs. 2 and 3 display the spectra of wavelet levels 1 to 8 for the solid cylinder and screen cylinder wakes respectively at all measured locations. Only the spectra of wavelet levels 1 to 8 are shown as the contributions to the measured velocity from wavelet levels higher than 8 is very small (only about 1% for

V-signals) at $x^* = 10$ in the solid cylinder wake. This will be used as the basis for comparing the different components in the different wake and also at different streamwise locations). The spectrum of each wavelet level displays a peak, which represents the central frequency. Each wavelet level covers a range of frequency. These central frequencies and their bandwidths are tabulated in Table I. These central frequencies correspond to the scales of turbulent structures. The higher the wavelet level, the lower the frequency bands indicating the larger the structures. It can be seen from both Fig. 2 and 3 that the most pronounced peaks that correspond to a certain wavelet level are distinctly obvious in both wakes, except in the screen cylinder wake at $x^* = 10$ (the most-pronounced peak in the solid cylinder wake at $x^* = 40$ is imperceptible due to the scale used in the Fig. 2). The central frequencies associated with the most pronounced peak in the solid cylinder wake correspond to the wavelet level 7 (Fig. 2) and in the screen cylinder wake, this correspond to level 6 (Fig. 3). These central frequencies coincide perfectly with the peak frequency of the measured v–signal. Thus, the central frequencies of wavelet level 7 (for solid cylinder) and level 6 (for screen cylinder) correspond to the dominant frequency f_o of the solid and screen cylinders at their respective downstream locations. These wavelet levels represent the organized large-scale structures located at the vortex shedding frequency.

The central frequency ratio (hereafter denoted as the frequency ratio) between the corresponding central frequency of each wavelet level and the dominant frequency, f_i/f_o, for both cylinders at different streamwise locations are also calculated and the average value is presented in Table I. Rinoshika and Zhou [8] performed a wavelet multiresolution analysis in a circular cylinder wake and based from their two-point velocity correlations and wavelet autocorrelation functions, they found that the f_o and $2f_o$ wavelet components displayed considerable two-dimensionality and concluded that the components were connected to the spanwise structures of large- and perhaps the intermediate-scale. The $4f_o$ structure was significantly less organized and highly three dimensional while those of $8f_o$ and higher did not show coherence, revealing the characteristics of incoherent structures. In addition, Li and Zhou [9] and Rinoshika and Zhou [10] compared the turbulent structures of the comparable scales between two wakes by using the same multiple of f_o between the wavelet components. They covered the scales from $1/2f_o$ to $8f_o$ that were the main concern in their analysis and characterized the scale $8f_o$ as the small-scale, $4f_o$ as the intermediate-scale and f_o as the large-scale structures. In Table I, it seems that the wavelet levels 1, 2 and 3 represent the small-scales for both wakes as the average frequency ratios of these levels at all locations are > 10 (in the solid cylinder wake) and > 7 (in the screen cylinder wake). Also, in both wakes, those of levels 4 and 5 represent the intermediate-scales (structures of frequency of about $2f_o - 5f_o$) while levels 6, 7 and 8 clearly indicate the large-scales (within and/or below f_o).
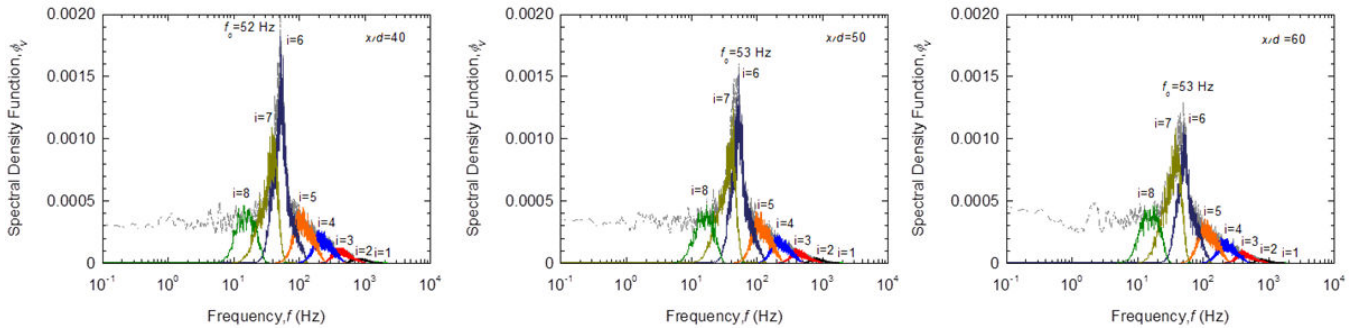
World Academy of Science, Engineering and Technology
International Journal of Mechanical and Mechatronics Engineering
Vol:8, No:2, 2014

Fig. 2 Spectra of the measured *v*-signals at *y/d*≈0.5 (dashed line) underlay the spectra of wavelet levels, *i*=1 to 8 of *v*-signals at *y/d*≈0.5 for solid cylinder at *x/d*=10, 20 and 40. The central frequency of wavelet level 7 (most pronounced peak) correspond to the dominant frequency, f_o
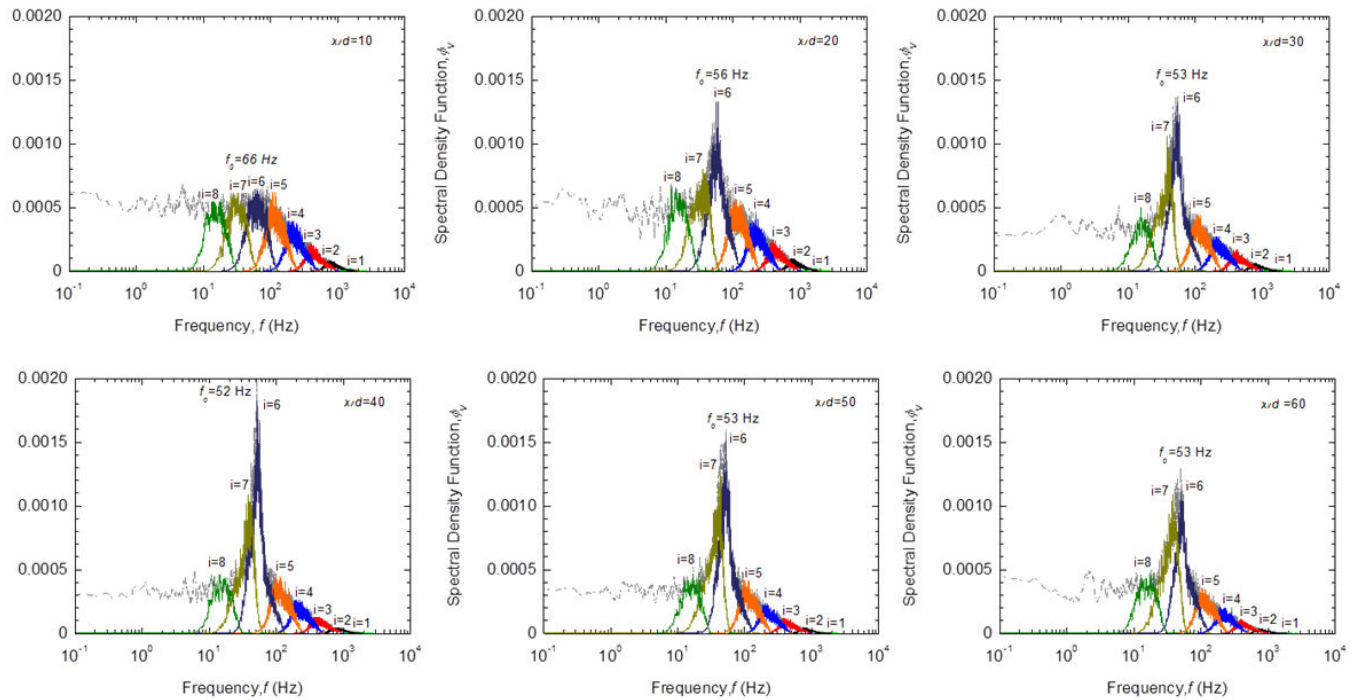

Fig. 3 Spectra of the measured *v*-signals at *y/d*≈0.5 (dashed line) underlay the spectra of wavelet levels, *i*=1 to 8 of *v*-signals at *y/d*≈0.5 for screen cylinder at *x/d*=10, 20, 30, 40, 50 and 60. The central frequency of wavelet level 6 (most pronounced peak) correspond to the dominant frequency, f_o

Referring back to Fig. 2, in the solid cylinder wake, it appears that wavelet components 7 and 6 are the only two components that are dominant throughout the wake although in the intermediate wake of $x^* = 40$, other structures can be seen to start gaining energy. It is evident that structures in the near-wake of the solid cylinder ($x^* = 10$ and 20) are dominated by the large-scales (levels 6 and 7) although the strength of these structures decay significantly with streamwise distance indicated by the decreased energy spectra in Fig. 2. It is interesting to highlight that in the near-wake of the screen cylinder at $x^* = 10$ (Fig. 3), the highly energetic behavior of the organized large-scale structures from level 6 is completely absent in comparison to the solid-cylinder wake at the same location; those of levels 4, 5, 7 and 8 are comparably dynamic. This reflects the different structures and shedding mechanism possessed by both wakes in which the former consists of primarily Kelvin-Helmholtz vortices as a result of the shear-layer instability while that in the latter consists of

Kármán vortices resulting from boundary layer separation from the cylinder [4]. Starting from $x^* = 20$, the large-scale structures of levels 6 and 7 start to dominate and those of other levels marginally decrease in strength, giving way to the large-scales. The strength of the wavelet components 6 and 7 both increases suddenly (from $x^* = 10$ to $x^* = 20$) and progressively ($x^* \geq 30$) before decreases only slightly at a particular location in the screen cylinder wake; these locations are at $x^* = 40$ for level 6 and at $x^* = 50$ for level 7. This behaviour seems to indicate the vortex merging and interactions between the structures of different scales, bringing about the occurrence of the large-scale vortices in the latter wake in comparison to the immediate near-wake location of the former. It is worthwhile mentioning that at $x^* \geq 40$, the spectral magnitudes for all other wavelet levels remain as if almost unchanged, implying the feeble interaction between the structures, thus resulting in the very slow decay of structures of the large-scales.

World Academy of Science, Engineering and Technology
International Journal of Mechanical and Mechatronics Engineering
Vol:8, No:2, 2014

TABLE I
CENTRAL FREQUENCIES AND BANDWIDTH OF EACH WAVELET LEVEL

Solid cylinder					
	Central frequency (Hz)			Average f_i/f_o	Frequency Bandwidth (Hz)
i	$x/d =10$	20	40		
1	1630	1480	1540	38	600-2800
2	766	766	766	19	300-2400
3	395	427	443	10	140-1200
4	208	193	233	5	70-600
5	98	98	99	2.4	35-300
6	47	47	53	1.2	18-140
7	$f_0 = 41$	**41**	**41**	**1**	**8-70**
8	16	19	16	0.4	4-35

Screen cylinder							
	Central frequency (Hz)						Avg f_i/f_o	Frequency Bandwidth (Hz)
i	10	20	30	40	50	60	
1	1480	1570	1559	1626	1590	1540	28	600-2800
2	758	788	783	824	827	788	14	300-2400
3	435	388	431	396	363	399	7	140-1200
4	240	235	231	244	202	229	4	70-600
5	109	107	106	110	99	107	2	35-300
6	**66**	**56**	**54**	**52**	**53**	**53**	**1**	**18-140**
7	33	36	39	40	43	36	0.7	8-70
8	18	12	17	17	21	18	0.3	4-35

C. Contributions to the Reynolds Normal Stresses from different Wavelet Components

The contributions from the turbulent motions of various scales to the velocity variances are calculated using

$$\langle \beta_i{}^2 \rangle = \frac{1}{k}\sum_{j=1}^{k} \beta_i{}^2 \qquad (5)$$

where k is the total number of data points and β_i represents the wavelet components of the fluctuating velocities u_i or v_i. The calculated $\langle \beta_i{}^2 \rangle$ is normalized by the maximum value, $(\langle \beta^2 \rangle)_{max}$, of the measured $\langle \beta^2 \rangle$ to compare the contribution from each component to the Reynolds normal stresses. The $(\langle \beta^2 \rangle)_{max}$ values are also tabulated in Table II. The values measured by Rinoshika and Zhou [10] for the circular cylinder and screen strip at $x/h = 20$ (h is the characteristic length) are also included in bracket. The values highlight discernible differences between the solid and screen cylinder wakes; the values of $(\langle u^2 \rangle)_{max}$ and $(\langle v^2 \rangle)_{max}$ are significantly higher in the former than that in the latter at their respective locations especially in the near-wake.

Figs. 4 to 7 show the lateral distributions of $\langle u_i^2 \rangle$ and $\langle v_i^2 \rangle$ at various wavelets as compared with the measured $\langle u^2 \rangle$ and $\langle v^2 \rangle$ values for the solid cylinder and screen cylinder wakes respectively at different streamwise locations. The total contributions from the wavelet components 1 to 8 to the total Reynolds normal stresses at $y^* = 0.5$ account for about

$69\% - 86\%$ of $\langle u^2 \rangle$ and $92\% - 98\%$ of $\langle v^2 \rangle$ in the solid cylinder wake, and $73\% - 95\%$ of $\langle u^2 \rangle$ and $95\% - 98\%$ of $\langle v^2 \rangle$ in the screen cylinder wake at the respective measured locations. In both wakes, the $\langle v_i^2 \rangle$ of components 1 to 8 accounts for about more than 92% to $\langle v^2 \rangle$, indicating that these 8 components are reasonable representative of the flow in terms of $\langle v^2 \rangle$ but not so in $\langle u^2 \rangle$.

For the solid cylinder (Fig. 4), the distributions of $\langle u_i^2 \rangle / (\langle u^2 \rangle)_{max}$ for wavelet levels 7 (structures at f_o) and 6 (structures at $1.2 f_o$) are similar to that of the measured data, especially at $x^* = 10$. The highest contribution to the measured variance comes from the large-scales structures (level 7 of about 40%), followed by level 6 (26%) at $x^* = 10$. These two levels are the most energy containing as depicted in the figure at all locations, consistent with the spectral plots (Fig. 2). At $x^* = 20$, these wavelet components accounts for almost the same contributions to the measured data (about 20%), particularly at $y^* < 0.7$. At $x^* = 40$, the contributions from these large-scale structures reduce and are almost similar near the centerline. It can be seen that, although the contribution from the organized large-scale structures (level 7) is the highest at $x^* = 10$, the effect from the wavelet component 6 is comparable to the wavelet component 7 at $x^* \geq 20$. In fact, the former slightly exceeds the latter near the centerline at $x^* = 20$. Apart from levels 7 and 6, the contributions from the small- and especially intermediate-scale structures may be appreciable farther down the wake of solid cylinder. The contributions from other small-scale structures (levels 1 and 2) seem insignificant. This is in-line with the findings of the breakdown of the large-scale vortices into relatively smaller-scale vortices with downstream distance.

TABLE II
THE MAXIMUM VALUE OF REYNOLDS NORMAL STRESSES RESULTS FROM [10] IS INCLUDED IN BRACKETS

Solid cylinder		
x/d	$(<u^2>)_{max}/U_\infty{}^2 \, x10^{-3}$	$(<v^2>)_{max}/U_\infty{}^2 \, x10^{-3}$
10	30	91.9
20	15.9[14.2]	31[25.3]
40	6.87	7.91
Screen cylinder [screen strip]		
10	4.45	6.05
20	6.26[4.9]	6.52[3.92]
30	3.96	4.73
40	3.25	5.83
50	2.74	4.64
60	2.38	3.79

World Academy of Science, Engineering and Technology
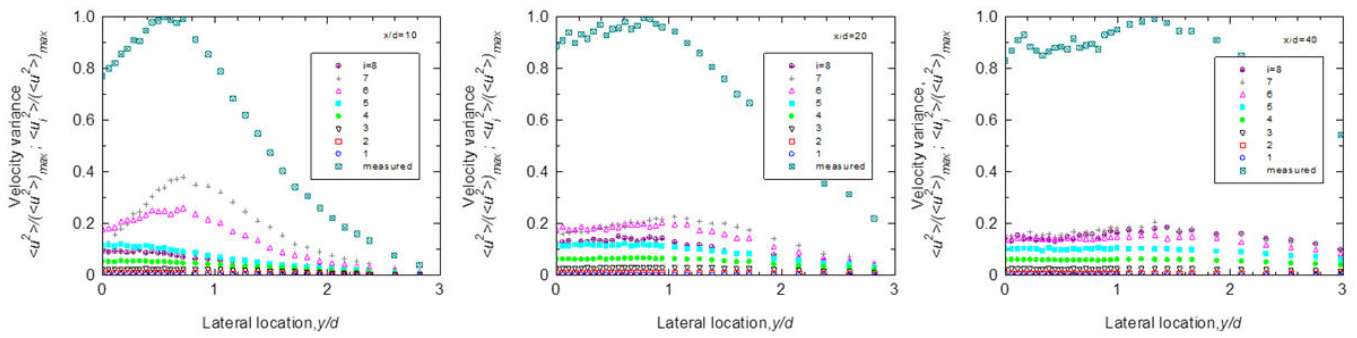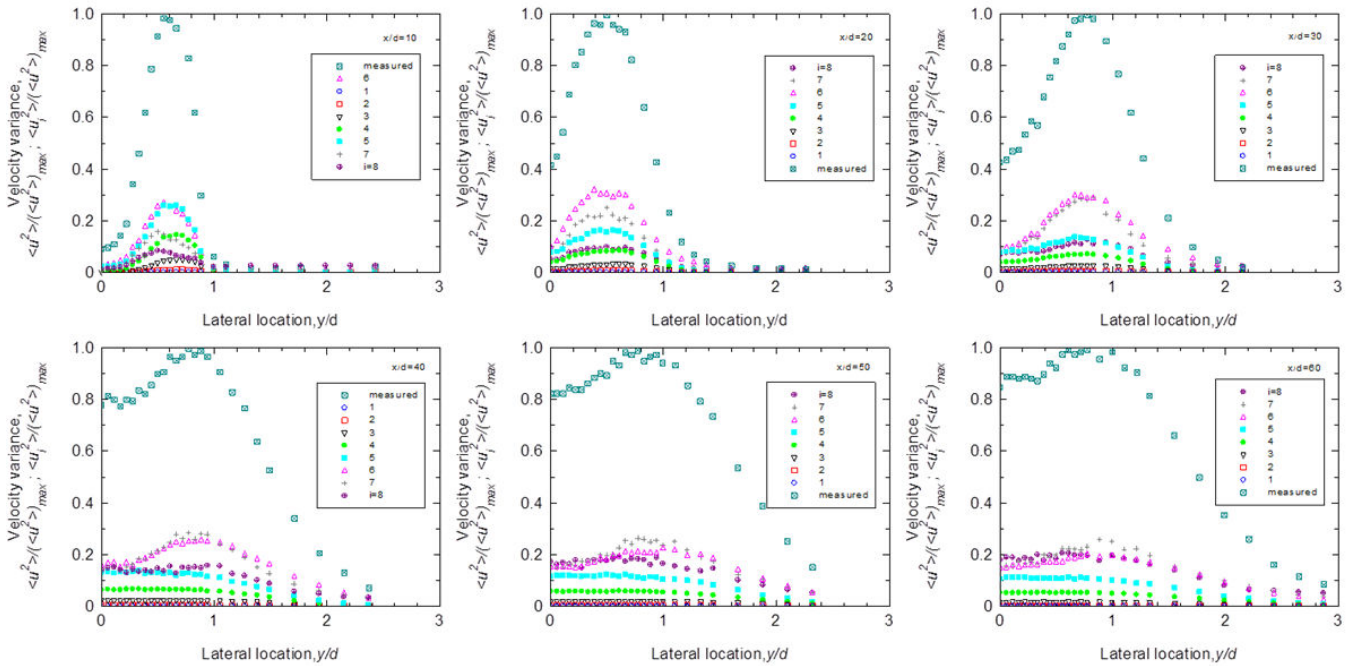International Journal of Mechanical and Mechatronics Engineering
Vol:8, No:2, 2014

Fig. 4 Velocity variance (normalized by the maximum value $<u^2>_{max}$) of the measured $<u^2>$ and wavelet components $<u_i^2>$ at various wavelet level for the solid cylinder wake at x/d =10, 20 and 40

Fig. 5 Velocity variance (normalized by the maximum value $<u^2>_{max}$) of the measured $<u^2>$ and wavelet components $<u_i^2>$ at various wavelet level for the screen cylinder wake at x/d =10, 20, 30, 40, 50 and 60

For the screen cylinder wake, the distributions of $\langle u_i^2 \rangle / (\langle u^2 \rangle)_{max}$ (Fig. 5) follow the measured data particularly at $x^* = 10 \rightarrow 30$. But at $x^* \geq 40$, the similar distributions to the measured data particularly those of small- and intermediate-scales disappear. The most significant contribution at $x^* = 10$ comes from wavelet levels 6 (organized large-scale structures at f_o) and 5 (intermediate-scale structures) with each comparably contributing about 26% to $(\langle u^2 \rangle)_{max}$, followed by levels 7 and 4 (17%). Other levels contribute less than 10% individually. This indicates that the intermediate structures of wavelet components 5 and 4 play a major role in the near-wake of the screen cylinder at $x^* = 10$ and this will further be demonstrated in the distributions of $\langle v_i^2 \rangle / (\langle v^2 \rangle)_{max}$ (Fig. 7) later. At $x^* = 20$, however, contributions from levels 5 and 4 drop significantly to 17% and 8%, respectively. Level 6 contributes the most at $x^* = 20$ (32%), indicating the significant role of the organized large-scale structures at this location, followed by level 7

(25%). At $x^* = 30$, the contributions from these two levels are almost equal. At $x^* > 40$, wavelet component level 7 exceeds level 6 to be the highest contributor, although very slightly. While the contributions to $(\langle u^2 \rangle)_{max}$ from level 6 decreases with x^* (after $x^* = 20$), those of levels 7 and 8 increase throughout the wake until $x^* = 30$ and at $x^* \geq 40$, the contributions from these two levels remains essentially the same. For $x^* \geq 50$, the contribution from level 8 exceeds that of level 6. The contributions from the small-scale structures (levels 1, 2 and 3) are negligible in the screen cylinder wake. Regarding the distributions of $\langle v_i^2 \rangle / (\langle v^2 \rangle)_{max}$ (Fig. 7), they follow closely the measured data, particularly those related with the large and intermediate-scale structures. Evidently, at $x^* = 10$, the role of the intermediate-scale structures of components 5 and 4 (correspond to about $2f_o$ and $4f_o$ respectively) can be clearly seen with a combined contributions of 49% to $(\langle v^2 \rangle)_{max}$ (27% from component 5 followed by 22% from component 4). Structures of component

World Academy of Science, Engineering and Technology
International Journal of Mechanical and Mechatronics Engineering
Vol:8, No:2, 2014

6 are also important (about 19%) to $(\langle v^2 \rangle)_{max}$ and the contribution from the organized structures is comparable to the intermediate-scales at about $y^* < 0.5$. The above results may imply that strong interactions between these structures are taking place and also reflect the different shedding mechanism from that of a solid cylinder. For $x^* \geq 20$, the organized large-scales structures of component 6 increases in energy and contribute the most to $(\langle v^2 \rangle)_{max}$, These structures are predominant and have the highest energy at $x^* = 40$ with a contribution of 54% compared to other locations. From $x^* > 40$, these structures slowly lose energy to make way for the

large structures of component 7 that also gradually gains energy thereafter. The intermediate-scale structures start to lose their roles down the wake as their contributions to $(\langle v^2 \rangle)_{max}$ decreases with x^*. The contributions from the small-scale structures of wavelet components 3, 2, 1 and the large-scale of component 8 also gradually drop with x^*. Notice also that for $x^* \geq 40$, the only two wavelet components that play substantial roles in the wake are from levels 6 and 7. The distributions of other levels remain practically the same at these locations.
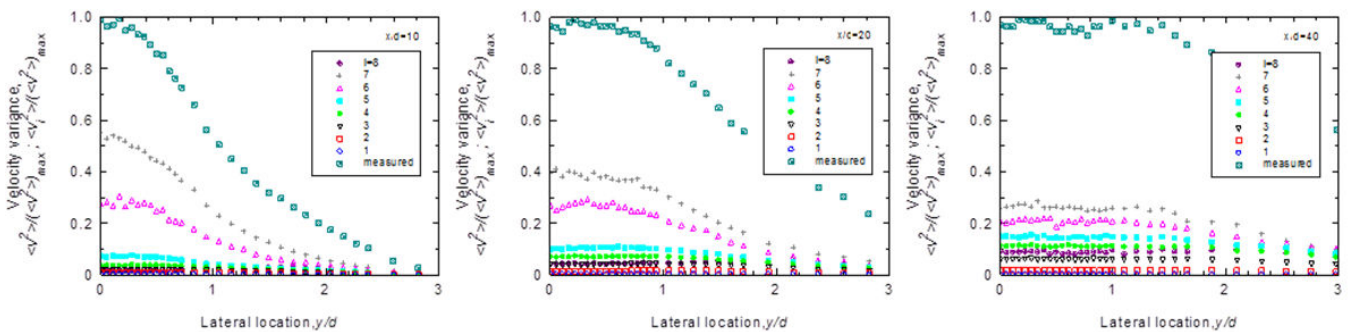

Fig. 6 Velocity variance (normalized by the maximum value $<v^2>_{max}$) of the measured $<v^2>$ and wavelet components $<v_i^2>$ at various wavelet level for the solid cylinder wake at x/d =10, 20 and 40
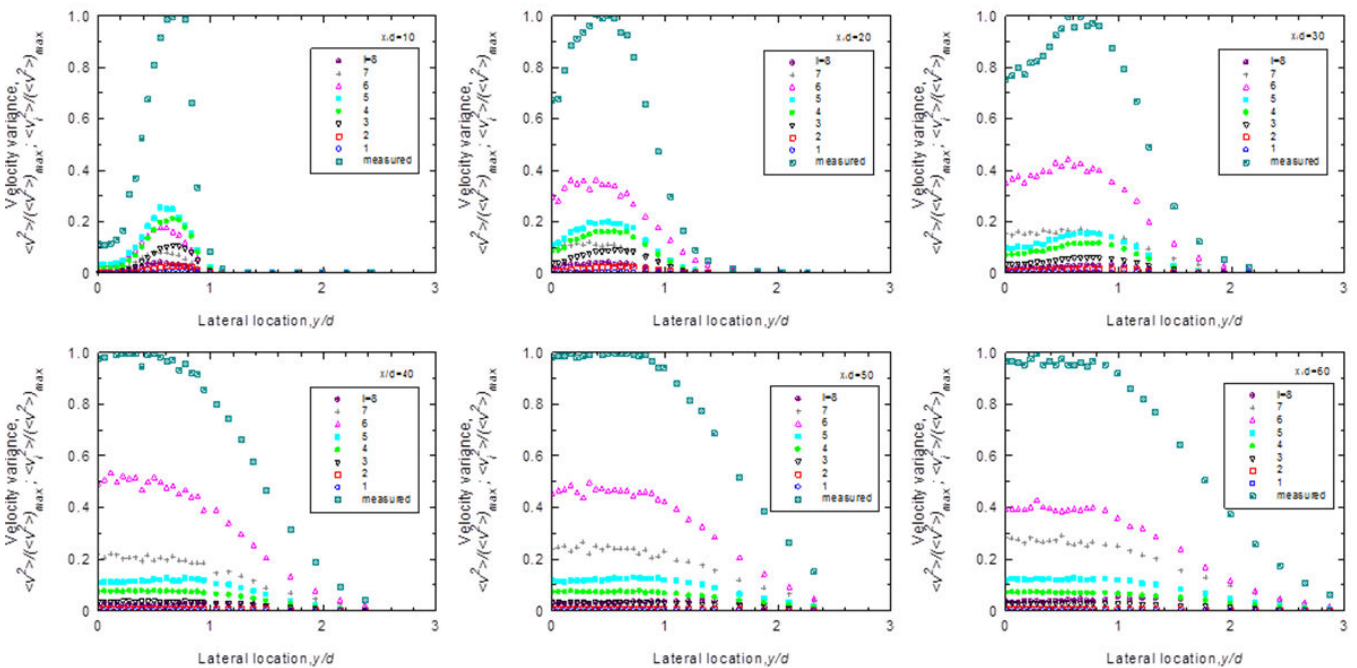

Fig. 7 Velocity variance (normalized by the maximum value $<v^2>_{max}$) of the measured $<v^2>$ and wavelet components $<v_i^2>$ at various wavelet level for the screen cylinder wake at x/d =10, 20, 30, 40, 50 and 60

While the large-scale structures of f_0 contribute the most to the total Reynolds stresses in the screen cylinder wake, the large-scale structures of f_0 and $1.2f_0$ jointly contribute in the solid cylinder wake. Rinoshika and Zhou [10] showed that in the solid cylinder wake at $x/h = x^* = 20$, the contribution to the Reynolds stresses were comparable from structures of f_0 and $2f_0$ whereby the combined contributions accounted for

about 43% and 74% to $(\langle u^2 \rangle)_{max}$ and $(\langle v^2 \rangle)_{max}$ respectively. In the present experiment, the combined contributions from structures of f_0 and $1.2f_0$ at $x^* = 20$ are about 40% and 71% to $(\langle u^2 \rangle)_{max}$ and $(\langle v^2 \rangle)_{max}$ respectively, reasonably similar to those in the former. It seems that the structures of $1.2f_0$ in the present experiment are comparable to the $2f_0$ structures in Rinoshika and Zhou [10]. In addition, these authors also

World Academy of Science, Engineering and Technology
International Journal of Mechanical and Mechatronics Engineering
Vol:8, No:2, 2014

reported significant contribution from the f_0 structures in the screen strip wake of 50% screen porosity at Re=5600, i.e. about 29% and 40% to $(\langle u^2 \rangle)_{max}$ and $(\langle v^2 \rangle)_{max}$ respectively. The contribution from the same scale structures in the screen cylinder wake is comparable to the former, about 32% and 38% to $(\langle u^2 \rangle)_{max}$ and $(\langle v^2 \rangle)_{max}$ respectively. It is relevant to remark that in the screen cylinder wake at $x^* = 20$, the maximum value of $\langle v_i^2 \rangle / (\langle v^2 \rangle)_{max}$ corresponding to the f_0 structures exceeds that of $\langle u_i^2 \rangle / (\langle u^2 \rangle)_{max}$, similar to the behaviour of the coherent contribution in the near-wake of a solid bluff-body [14]. In fact, at $x^* \geq 30$, the screen cylinder wake displays the same behaviour of $\langle v_i^2 \rangle / (\langle v^2 \rangle)_{max} > \langle u_i^2 \rangle / (\langle u^2 \rangle)_{max}$ whereby the largest difference between $\langle v_i^2 \rangle / (\langle v^2 \rangle)_{max}$ and $\langle u_i^2 \rangle / (\langle u^2 \rangle)_{max}$ is found at $x^* = 40$ (about 52% difference). Interestingly, however, at $x^* = 10$, the behaviour of structures at f_0 in the screen cylinder wake is opposite to those of other downstream locations, i.e. $\langle u_i^2 \rangle / (\langle u^2 \rangle)_{max} > \langle v_i^2 \rangle / (\langle v^2 \rangle)_{max}$, resembling the behaviour of coherent contribution in the turbulent far-wake [15]. This implies that the f_0 structures only start to become apparent at $x^* \geq 20$ but are most significant at $x^* = 40$, signifying a much longer vortex formation process.

V. CONCLUSION

The wake generated by a screen cylinder has been examined using the wavelet multiresolution technique in order to study the characteristics and behavior of turbulence structures of various scales and their evolution in the streamwise direction. The results are compared with that of a solid cylinder. The contributions to the Reynolds from various scales have also been calculated. The following can be drawn.

1) In the solid cylinder wake, the large-scale structures of f_o (component 7) and $1.2f_o$ (component 6) are the two most energetic structures throughout the wake, although the strength of the f_o structures are largely enervated at $x^* = 40$, consistent with the fast decay of the vortex strength as x^* increases [16]. This is in apparent different to that in the screen cylinder wake, whereby at $x^* = 10$, the intermediate- and the organized large-scale structures are comparably energetic but starting from $x^* \geq 20$, the f_o structures (component 6) increases in strength until $x^* = 40$ and followed by a slow decay thereafter.

2) The most significant contributions to the Reynolds stresses come from the f_o and $1.2f_o$ structures throughout the solid cylinder wake even though the f_o contribution drops significantly by about 50% at $x^* = 40$ where the intermediate-scale structures start to dominate in the solid cylinder wake. In the screen cylinder wake, the f_o structures are dominant and give the most contributions to the Reynolds stresses at $x^* \geq 20$, with the highest contribution to $(\langle v^2 \rangle)_{max}$ being seen at $x^* = 40$ (54%) before contributing slightly less thereafter, but not so at $x^* = 10$, where the intermediate-scale structures (components 5 and 4) contribute the most.

3) The wavelet analysis reflects the existence of different structures as well as the different formation mechanism in

the two wakes. The screen cylinder wake shows a longer formation of large-scale vortices at $x^* = 20$ followed by a slow decay of coherent vortices at $x^* > 40$, a contrast to that of a solid cylinder wake which shed large-scale vortices immediately in the wake that greatly decay downstream.

REFERENCES

[1] R. D. Blevins, *Flow-induced vibration*, 2nd ed. New York: Van Nostrand Reinhold, 1990.
[2] P. Price, "Suppression of the flow-induced vibration of circular cylinders," *J. Eng. Mech. Div., Am. Soc. Civ. Eng.,* vol. 82, 1956.
[3] M. M. Zdravkovich and J. R. Volk, "Effect of shroud geometry on pressure distributed around a circular cylinder," *Journal of Sound and Vibration,* vol. 20, pp. 451-455, 1972.
[4] A. M. Azmi, T. Zhou, H. Wang, L. P. Chua, and L. Cheng, "On the effectiveness and mechanism of vortex induced vibration suppression using a screen cylinder," in *Twenty-second (2012) International Offshore and Polar Engineering Conference*, Rhodes, Greece, 2012, pp. 586-594.
[5] M. Farge, "Wavelet Transforms and Their Applications to Turbulence," *Annual Review of Fluid Mechanics,* vol. 24, pp. 395-457, 1992.
[6] M. Farge and G. Rabreau, "Wavelet Transform to Detect and Analyze Coherent Structures in Two-Dimensional Turbulent Flows," *Comptes Rendus De L Academie Des Sciences Serie Ii,* vol. 307, pp. 1479-1486, Oct 30 1988.
[7] C. Meneveau, "Analysis of Turbulence in the Orthonormal Wavelet Representation," *Journal of Fluid Mechanics,* vol. 232, pp. 469-520, Nov 1991.
[8] A. Rinoshika and Y. Zhou, "Orthogonal wavelet multi-resolution analysis of a turbulent cylinder wake," *Journal of Fluid Mechanics,* vol. 524, pp. 229-248, Feb 10 2005.
[9] H. Li and Y. Zhou, "Comparison between triangular cylinder and screen near-wakes in the orthogonal wavelet representation," *Jsme International Journal Series B-Fluids and Thermal Engineering,* vol. 46, pp. 366-376, Aug 2003.
[10] A. Rinoshika and Y. Zhou, "Effects of initial conditions on a wavelet-decomposed turbulent near-wake," *Physical Review E,* vol. 71, Apr 2005.
[11] A. Rinoshika and Y. Zhou, "Effects of initial conditions on wavelet-decomposed structures in a turbulent far-wake," *International Journal of Heat and Fluid Flow,* vol. 28, pp. 948-962, 2007.
[12] S. F. M. Razali, T. Zhou, A. Rinoshika, and L. Cheng, "Wavelet analysis of the turbulent wake generated by an inclined circular cylinder," *Journal of Turbulence,* vol. 11, pp. 1-25, May 11 2010.
[13] I. Daubechies, "Ten lectures on wavelets," 1992.
[14] Y. Zhou and R. A. Antonia, "Critical-Points in a Turbulent near Wake," *Journal of Fluid Mechanics,* vol. 275, pp. 59-81, Sep 25 1994.
[15] Y. Zhou and R. A. Antonia, "Memory effects in a turbulent plane wake," *Experiments in Fluids,* vol. 19, pp. 112-120, Jun 1995.
[16] Y. Zhou and R. A. Antonia, "A Study of Turbulent Vortices in the near Wake of a Cylinder," *Journal of Fluid Mechanics,* vol. 253, pp. 643-661, Aug 1993.